PHYSICAL REVIEW E **71**, 035201(R) (2005)

Synchronization of non-phase-coherent chaotic electrochemical oscillations

István Z. Kiss, Qing Lv, and John L. Hudson
Department of Chemical Engineering, 102 Engineers' Way, University of Virginia, Charlottesville, Virginia 22904-4741, USA
(Received 25 October 2004; published 11 March 2005)

Experiments on phase and generalized synchronization of two coupled, nonidentical chaotic electrochemical oscillations are presented. We adapt measures of characterizing synchronization of a non-phase-coherent chaotic behavior and compare its properties and physicochemical mechanism to those of a phase-coherent behavior. Phase synchronization sets in along with the onset of generalized synchronization for the non-phase-coherent oscillations in contrast to phase-coherent oscillations in which the phase synchronization usually occurs at a weaker coupling strength.

DOI: 10.1103/PhysRevE.71.035201 PACS number(s): 05.45.Xt, 82.40.Np

Synchronization of coupled chaotically oscillating systems has received considerable recent interest [1]. Most studies are done with phase-coherent oscillations in which phase and amplitude are easily defined and in which the variance of instantaneous periods is small yielding a relatively narrow peak in the Fourier transform [2]. In such systems phase synchronization (bounded phase difference [1]) occurs at much smaller coupling strengths [3] than identical [4] or generalized synchronization (continuous functional relationship between attractors) [5]. There are many experimental examples of coupling and forcing of phase-coherent chaotic systems in physics [6], chemistry [7], and biology [8,9].

However, many systems are non-phase-coherent and a principal frequency is not easily defined; they exhibit higher complexity and can have more than one characteristic time scale [10]. Examples are seen in lasers [11], fluid flow [12], and chemical oscillations [13]. Multiple time scales are inherent in physiologic dynamics [14]. Non-phase-coherent oscillations can be a sign of dysfunction. Highly irregular oscillations with a broad power spectrum have been reported for spontaneously hypertensive rats [15]. Non-phase-coherent systems impose two challenges. First, the definitions of instantaneous phase and amplitude are not straightforward; several approaches have been proposed using wavelets [11,15,16], an external nonlinear locking device [13], or a method based on curvature of the trajectory in state space [10]. Second, the synchronization differs from the phase-coherent case; theoretical and simulation studies have shown that phase and generalized synchronization can both occur at strong coupling strengths in systems with non-phase-coherent attractors [10], in systems with large heterogeneities [17], or in the coupling of disparate oscillators [18].

In this paper we compare synchronization of coupled non-phase-coherent and phase-coherent chaotic systems using two laboratory model systems from electrochemistry. The first is iron electrodissolution which exhibits bistability, periodic oscillations, and chaos depending on parameters such as applied potential, external resistance, and rate of mass transfer to the surface [19]. In the parameter range considered in this paper the electrodissolution undergoes complex chaotic behavior for which standard methods of phase definitions fail. Phases of the oscillations are calculated with a method based on trajectory curvature [10], and a measure of phase synchronization [9] is obtained as a function of the coupling strength. Generalized synchronization is quantified with a test of functional relationship between the two coupled systems using an algorithm based on a method of false neighbors [20]. The coupling strength at which phase and generalized synchronization occurs is determined and compared to results obtained with the coherent chaotic electrodissolution of nickel [7].

A standard three-compartment electrochemical cell consisting of two iron working electrodes (1-mm diameter each with 2-mm spacing), a $Hg/Hg_2SO_4/K_2SO_4$ reference electrode, and a Pt mesh counter-electrode was used. (A schematic of the experimental setup can be found in Ref. [7].) The applied potential (V) of both electrodes was held at the same value. The electrodes were connected to the potentiostat through two individual parallel resistors (R_{ind}) and through one series collective resistor (R_{coll}) which furnishes a global coupling of strength $\varepsilon = R_{coll}/R_{tot}$, where $R_{tot} = R_{coll} + R_{ind}/2$ is kept constant. For $\varepsilon = 0$, the external resistance furnishes no additional coupling; for $\varepsilon = 1$, maximal external coupling is achieved [7].

Both relatively slow and fast cycles are seen in the current time series and the reconstructed attractor shows no obvious center of rotation as shown in Figs. 1(a) and 1(b), respectively. The phase $[\phi(t)]$ can be defined using the derivative of the Hilbert transform $H(t)$ of the current $i(t)$

$$\phi(t) = \arctan \frac{dH(t)/dt}{di(t)/dt}. \quad (1)$$

Osipov *et al.* have previously proposed the use of a two-dimensional phase space based on derivative component coordinates [10]. Although there is no unique center of rotation in the phase space using the Hilbert transform [21] [Fig. 1(c)], a unique center is found using the derivative of both coordinates [Fig. 1(d)]; thus Eq. (1) can be used for the definition of phase. The extent of phase coherence can also be seen in the return times of the time series data. While for the phase-coherent chaos of Ni electrodissolution the oscillations have similar return times (±10%) [see Fig. 2(a)], for the non-phase-coherent chaos of iron dissolution [see Fig. 2(b)] oscillations with very small and large periods occur. It is also seen in the figure that this behavior is stationary; the large changes are not due to drift but due to a dynamic process.

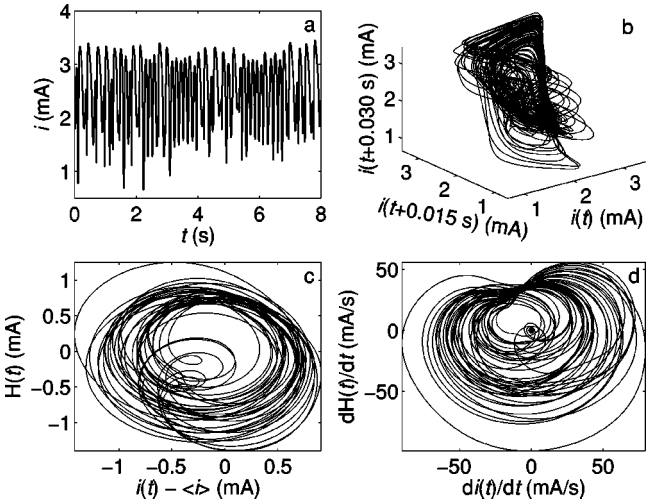

FIG. 1. Dynamics of a single electrode. (a) Time series of the current. (b) Attractor using time-delay coordinates. (c) Phase space using the Hilbert transform. (d) Phase space using the derivative of the Hilbert transform. (Black circle at the origin denotes the center of rotation.)

(We have also confirmed the stationarity of oscillations with a wavelet-based method [22]; the wavelet analysis shows only small fluctuations in characteristic frequencies but no long-term drift).

Without added coupling ($\varepsilon=0$) the two-electrode results are shown in Fig. 3. The current of electrode 1 vs electrode 2 [Fig. 3(a)] does not show any obvious correlation. Phases are obtained with Eq. (1) and phase differences defined as $\Delta\phi(t)=\phi_1(t)-\phi_2(t)$. The magnitude of phase differences tends to increase with time [see Fig. 3(b)]; however, large fluctuations from a straight line occur due to the strong non-phase-coherent feature of the chaotic oscillations. (These fluctuations are much smaller for the phase-coherent chaotic Ni electrodissolution [7].) The histogram of the cyclic phase differences ($\Delta\phi \bmod 2\pi$) [Fig. 3(c)] is flat, indicating no favored phase difference and no significant inherent coupling at $\varepsilon=0$ through the electrolyte. A synchronization index σ can be used to quantitatively characterize the extent of phase synchronization [9]; the value of σ expresses the sharpness of the maximum in the cyclic phase difference distribution and is obtained as

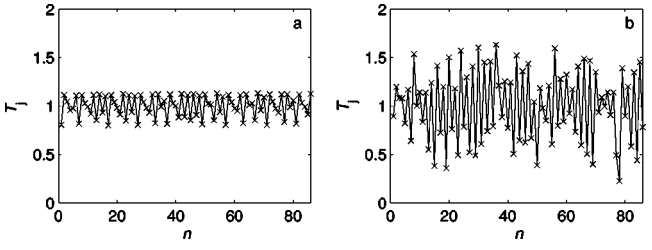

FIG. 2. Time series of dimensionless return times, $T_j=t_j/\langle t_j\rangle$, where t_j is the time between two maxima in current time series. (a) Ni dissolution with phase coherent chaos (time series data taken from Ref. [7]). (b) Iron dissolution with non-phase-coherent chaos (conditions are given in Fig. 1).

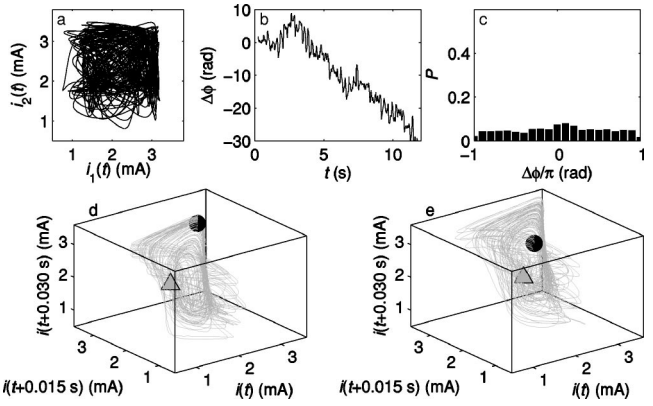

FIG. 3. Two non-phase-coherent chaotic systems without added coupling ($\varepsilon=0$, $V=-0.321$ V). (a) Current of electrode 2 vs electrode 1. (b) Phase difference vs time. (c) Histogram of cyclic phase difference ($\Delta\phi \bmod 2\pi$ modulated into $[-\pi,\pi]$). (d) and (e) Reconstructed attractors of the electrodes using time-delay coordinates. The circles represent phase points at an arbitrary time; triangles represent nearest-neighbor image points.

$$\sigma=(S_{\max}-S)/S_{\max}, \tag{2}$$

where S is the Shannon entropy of the cyclic phase difference distribution ($S=-\sum_{i=1}^{M}p_i \ln p_i$, M is the number of bins in the histogram of cyclic phase differences in Fig. 3(c), p_i is the fraction of data points in the ith bin), and $S_{\max}$ is the maximum entropy (flat distribution). σ takes on values from 0 to 1 as the distribution changes from flat to a delta function. For $\varepsilon=0$ in Fig. 3(c), $\sigma=0.008$.

Generalized synchronization can be characterized with a quantity that expresses a continuous functional relationship between the attractors of the two systems [5]. Continuity was difficult to prove (even for two identical systems); however, a robust algorithm based on false nearest neighbors has been proposed to characterize functional relationships between signals [20]. The method was developed to determine optimal embedding dimension and time delay. Nevertheless, as we shall see below, it provides an efficient way to characterize generalized synchronization as well. At any time t^* the phase points of electrode one and two are $\mathbf{x}_1(t^*)$ and $\mathbf{x}_2(t^*)$. The nearest neighbors of these two points, $\mathbf{x}_1(t_1)$ and $\mathbf{x}_2(t_2)$, respectively, are determined (with the software package OPENTSTOOL [23]). Functional relationships are assumed to exist if both $|\mathbf{x}_2(t^*)-\mathbf{x}_2(t_1)|<\delta$ and $|\mathbf{x}_1(t^*)-\mathbf{x}_1(t_2)|<\delta$ are fulfilled, where $\delta=0.7$ mA. The reconstruction of the attractors was done using the method of time delays with the current $[i(t)]$ signal of the electrodes; reconstruction parameters (time delay, $\tau=0.015$ s and embedding dimension, $m=4$) were determined in such a way to avoid false neighbors [20]. The functional relationship between the electrodes is characterized by the fraction of phase points P that passes the false neighbor test. An example is shown in Figs. 3(d) and 3(e). The large distances between the phase points at t^* (circles) and at t_1 and t_2 (triangles), respectively, show that there is no functional relationship between the two phase points at $t=t^*$. The analysis of the whole time series at $\varepsilon=0$ gives P

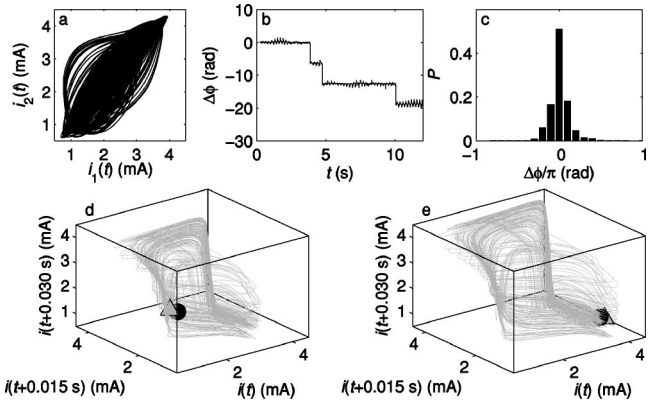

FIG. 4. Two non-phase-coherent chaotic systems with added coupling ($\varepsilon=0.6$, $V=-0.300$ V). (a) Current of electrode 2 vs electrode 1. (b) Phase difference vs time. (c) Histogram of cyclic phase difference ($\Delta\phi \bmod 2\pi$ modulated into $[-\pi,\pi]$). (d) and (e) Reconstructed attractors of the electrodes using time-delay coordinates. The circles represent phase points at an arbitrary time; triangles represent nearest-neighbor image points.

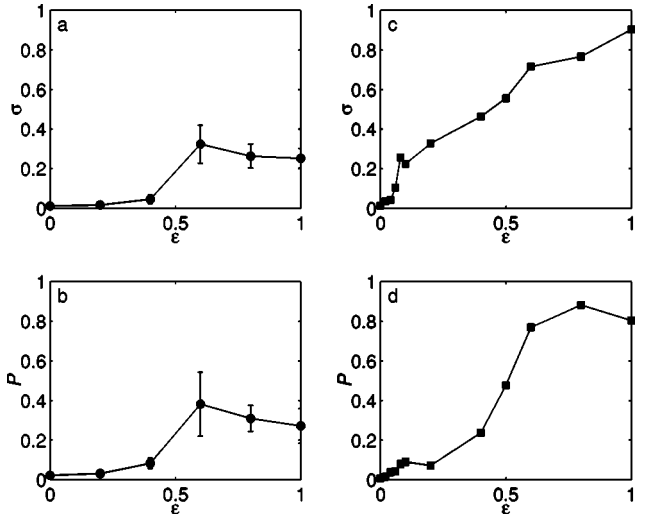

FIG. 5. Phase and generalized synchronization of non-phase-coherent and phase-coherent systems. Left column: a non-phase-coherent system in iron electrodissolution. Error bars indicate standard deviation of data obtained in nine experiments for -0.36 V $\leqslant V \leqslant -0.18$ V. (a) The synchronization index as a function of coupling strength. (b) The fraction of phase points passing the nearest-neighbor test vs coupling strength. Right column: the phase-coherent chaotic system of Ni dissolution. (c) The synchronization index as a function of coupling strength. (d) The fraction of phase points passing the nearest-neighbor test vs coupling strength ($m=3$, $\tau=0.1$ s, $\delta=0.01$ mA).

$=0.004$, i.e., only a small fraction (0.4%) of the phase points passes the false neighbor test.

Now we consider the addition of fairly strong coupling ($\varepsilon=0.6$, Fig. 4). With this added coupling there is a remarkable change in the synchronization properties of the oscillations. Although identical synchronization (corresponding to the diagonal line) in the $i_1(t)$ vs $i_2(t)$ plot [Fig. 4(a)] is not present, there is correlation between the currents of the electrodes. The phase differences [Fig. 4(b)] are nearly constant with some phase slips (these are related to sharp peaks in time series for which state space reconstruction is inaccurate). The histogram of cyclic phase differences [Fig. 4(c)] has a maximum near zero; antiphase oscillations are practically not observed, i.e., the probabilities at $-\pi$ and π differences are almost zero. The synchronization index has a large value $\sigma=0.412$; our previous studies showed that phase synchronization is established when $\sigma>0.1-0.2$ [7]. Thus, we see that the phases of the oscillations are correlated and at $\varepsilon=0.6$ phase synchronization has set in.

The phase points of the attractors shown in Figs. 4(d) and 4(e) pass the nearest-neighbor test. Note that the corresponding phase points (shown in triangles and circles) reside on different parts of the two attractors; such a mapping is indicative of generalized synchronization. The analysis gave $P=0.456$ showing that about half of the phase points pass the false neighbor test.

The synchronization index σ and the fraction of data points that pass the neighbor tests (P) are shown as a function of the coupling strength in Figs. 5(a) and 5(b). The figures show a similar trend with a large increase in the values of σ and P between $\varepsilon=0.4$ and 0.6. (There is small increase of these quantities for $\varepsilon<0.4$.) These results imply that phase and generalized synchronization occur in a parallel way in the system as the coupling strength is varied.

Similar experiments with two chaotic systems with varying coupling strength were carried out with nickel electrodissolution [7]. In this system the chaotic attractor is phase coherent and phase synchronization was previously shown to occur at $\varepsilon=0.06$. In Figs. 5(c) and 5(d) σ and P are shown as a function of coupling strength. Phase synchronization sets in at $\varepsilon=0.06$ at which coupling strength σ increases considerably. Generalized synchronization sets in at about $\varepsilon=0.5$ as shown by the large increase of P. Thus, for phase-coherent chaotic oscillations, phase and generalized synchronization are distinct processes occurring at weak and strong coupling strength, respectively.

Depending on the coherence of the chaotic attractor three types of transitions have been proposed—from unsynchronized to both phase and generalized synchronized states [10]. For phase-coherent attractors the zero Lyapunov exponent (LE) is associated with the phase dynamics and phase synchronization occurs at weak coupling shortly after the zero LE becomes negative and generalized synchronization occurs at the strong correlation of amplitudes at large coupling; apparently, the transition seen in Ni electrodissolution belongs to this category. For chaotic attractors with intermediate phase diffusion the transition takes place via an interior crisis. For strongly non-phase-coherent attractors phase synchronization is a manifestation of generalized synchronization and phase synchronization occurs only after one of the positive LE passes to negative values, i.e., transition to generalized synchronization. In this case phase locking is possible only with strong correlations of the amplitudes. Iron electrodissolution was shown to fall into this category; the measures for phase and generalized synchronization followed the same trend of variations.

Although detailed differential equation models of chaotic

nickel and iron oscillations are not available, the general mechanism for the development of oscillations is known. Chaotic nickel dissolution with a phase coherent attractor can develop through period-doubling bifurcations and the system can be modeled with three variables: potential, and NiO and NiOH surface coverages [24]. However, to capture the basic dynamical features of iron dissolution at least four variables are required [25]; one of them is a slowly varying salt layer thickness. It is likely that this slow variable contributes to the large phase incoherent character of the oscillations.

Two main routes to phase and generalized synchronization have been confirmed in laboratory experiments with electrochemical systems. Depending on the phase-coherent features, phase and generalized synchronization can be independent or highly correlated processes. The robustness of the analysis method applied here can be useful for characterizing other physical, chemical, and biological systems that are composed of oscillations with different degrees of coherence. For example, in an analysis of rat electroencephalographic signals [26] measures of phase and generalized synchronization exhibited similar trends that imply underlying non-phase-coherent dynamics.

This work was supported by the National Science Foundation (Contract No. CTS-0317762).

[1] A. S. Pikovksy, M. G. Rosenblum, and J. Kurths, *Synchronization: A Universal Concept in Nonlinear Science* (Cambridge University Press, Cambridge, 2001); M. G. Rosenblum, A. S. Pikovsky, and J. Kurths, Phys. Rev. Lett. **76**, 1804 (1996).
[2] E. F. Stone, Phys. Lett. A **163**, 367 (1992).
[3] U. Parlitz *et al.*, Phys. Rev. E **54**, 2115 (1996).
[4] H. Fujisaka and T. Yamada, Prog. Theor. Phys. **69**, 32 (1983); A. S. Pikovsky and P. Grassberger, J. Phys. A **24**, 4587 (1991); L. M. Pecora and T. L. Carroll, Phys. Rev. Lett. **64**, 821 (1990).
[5] N. F. Rulkov *et al.*, Phys. Rev. E **51**, 980 (1995).
[6] N. F. Rulkov, Chaos **6**, 262 (1996); P. M. Varangis *et al.*, Phys. Rev. Lett. **78**, 2353 (1997); E. Rosa *et al.*, Int. J. Bifurcation Chaos Appl. Sci. Eng. **10**, 2551 (2000).
[7] I. Z. Kiss and J. L. Hudson, Phys. Chem. Chem. Phys. **4**, 2638 (2002); I. Z. Kiss, W. Wang, and J. L. Hudson, *ibid.* **2**, 3847 (2000).
[8] C. Schäfer *et al.*, Nature (London) **392**, 239 (1998).
[9] P. Tass *et al.*, Phys. Rev. Lett. **81**, 3291 (1998).
[10] G. V. Osipov *et al.*, Phys. Rev. Lett. **91**, 024101 (2003).
[11] D. J. DeShazer *et al.*, Phys. Rev. Lett. **87**, 044101 (2001).
[12] D. Maza *et al.*, Phys. Rev. Lett. **85**, 5567 (2000); **86**, 3213(E) (2001).
[13] M. G. Rosenblum *et al.*, Phys. Rev. Lett. **89**, 264102 (2002).
[14] M. Costa, A. L. Goldberger, and C. K. Peng, Phys. Rev. Lett. **89**, 068102 (2002); N. Wessel, A. Schirdewan, and J. Kurths, *ibid.* **91**, 119801 (2003).
[15] O. V. Sosnovtseva *et al.*, Phys. Rev. E **66**, 061909 (2002).
[16] J. P. Lachaux *et al.*, Int. J. Bifurcation Chaos Appl. Sci. Eng. **10**, 2429 (2000).
[17] Z. G. Zheng and G. Hu, Phys. Rev. E **62**, 7882 (2000).
[18] S. Bowong and F. M. M. Kakmeni, Phys. Scr. **68**, 326 (2003).
[19] J. L. Hudson and T. T. Tsotsis, Chem. Eng. Sci. **49**, 1493 (1994).
[20] C. L. Goodridge *et al.*, Phys. Rev. E **64**, 026221 (2001); S. Boccaletti *et al.*, *ibid.* **65**, 035204(R) (2002).
[21] A. S. Pikovsky *et al.*, Physica D **104**, 219 (1997).
[22] M. Bracic and A. Stefanovska, Bull. Math. Biol. **60**, 919 (1998).
[23] C. Merkwirth *et al.*, OPENTSTOOL, http://www.physik3.gwdg.de/tstool/index.html.
[24] D. Haim *et al.*, J. Phys. Chem. **96**, 2676 (1992).
[25] L. Organ, I. Z. Kiss, and J. L. Hudson, J. Phys. Chem. B **107**, 6648 (2003).
[26] R. Quian Quiroga *et al.*, Phys. Rev. E **65**, 041903 (2002).